September 1986 LRP 306/86

BROADBAND MAGNETIC AND DENSITY FLUCTUATIONS IN THE TCA TOKAMAK

Ch. Hollenstein, R. Keller, A. Pochelon, F. Ryter,
M.L. Sawley, W. Simm and H. Weisen

Invited Paper presented by A. Pochelon at
the International Workshop on
Small Scale Turbulence and Anomalous Transport in Magnetized Plasmas
Cargèse (Corsica, France)
6 - 12 July 1986

BROADBAND MAGNETIC AND DENSITY FLUCTUATIONS IN THE TCA TOKAMAK

Ch. Hollenstein, R. Keller, A. Pochelon, F. Ryter, M.L. Sawley, W. Simm and H. Weisen

Centre de Recherches en Physique des Plasmas
Association Euratom - Confédération Suisse
Ecole Polytechnique Fédérale de Lausanne
21, Av. des Bains, CH-1007 Lausanne/Switzerland

ABSTRACT

The results of comparative studies of broadband magnetic and density fluctuations during ohmic discharges in the TCA tokamak are described. Long coherence lengths are observed in poloidal and toroidal directions between magnetic probes in the scrape-off layer. A phase contrast diagnostic provides a newly accessible range of density fluctuations in the bulk plasma with very long wavelengths. Langmuir probes provide similar measurements in the scrape-off layer. Statistical dispersion relations for both density and magnetic fluctuations are deduced and are shown to be substantially different. Low mean poloidal wavenumbers (m ~2 at 100 kHz) are obtained for the magnetic fluctuations, in contrast to the much higher values measured for density fluctuations. The difference between magnetic and density fluctuations is also reflected in different scalings with plasma parameters and with electron confinement time. The helicity of the coherent magnetic structures is analyzed to show that interior regions of the plasma, such as the q = 2 region, contribute to the magnetic activity at the edge. This explains why the magnetic fluctuations measured at the edge are likely to reflect the confinement properties of the bulk plasma. The results of detailed probe rotation experiments and coherence measurements give indications of the physical nature and origin of magnetic fluctuations.

INTRODUCTION

Energy and particle transport in tokamaks are much higher than predicted from neoclassical theory, and are generally believed to be associated with the presence of plasma turbulence [1]. Laser scattering experiments that measure broadband density fluctuations [e.g. 2-4] have received considerable attention since they can provide information about the bulk plasma. In addition, measurements have been made using Langmuir and magnetic probes located in the scrape-off plasma [e.g. 5-9]. Although it has sometimes been suggested that such measurements only provide information about the edge plasma, it is now recognized that the edge plasma may play an important role in determining the confinement properties of the bulk plasma [10]. In addition, since magnetic probes provide a nonlocal measurement of fluctuating plasma currents, magnetic fluctuations may give an indication of more global properties.

An understanding of the physical nature and origin of broadband density and magnetic fluctuations can be obtained from a knowledge of their statistical dispersion relations. The dispersion relations can be experimentally determined using correlation techniques analyzing signals measured at different spatial locations. In the present paper, a detailed study of density and magnetic fluctuations in a tokamak is presented. Comparisons are made between the measurements of spectra, scaling with plasma parameters and spatial correlations, providing better insights into the nature of the fluctuations and their role in confinement.

EXPERIMENTAL DETAILS

All the data described here have been obtained from ohmically-heated discharges of the TCA tokamak.

The parameters of the TCA tokamak are:

$R/a = 0.61m/0.18m = 3.4$

$B_\phi \leq 1.5$ T

$I_p < 175$ kA, flat top $\lesssim 0.15$ sec.

$T_{eo} \sim 700$ eV, $T_{io} \sim 300$ eV

The tokamak was equipped with four poloidal SiC-coated carbon limiters located at one toroidal location. Unless otherwise specified, the data presented in this paper were obtained from "standard" discharges with B_ϕ = 1.5 T, q(a) = 3.2 and $\bar{n}_e$ = 2.5 10^{19} m^{-3}. Constant plasma current and density were maintained during the time data were taken, to ensure stationary conditions.

Apart from the usual tokamak diagnostics (Fig. 1), the present study makes particular use of the following diagnostics: 1) magnetic probes placed at several different locations in the shadow of the limiters; 2) a CO_2-phase contrast diagnostic for density fluctuation measurements; and 3) a triple Langmuir probe located ~180° toroidally from the limiters.

The magnetic probe system comprises two triple probes and a poloidal array of ten single probes. The triple probes (b_r, b_θ, b_ϕ) are located 180° toroidally apart, one on the top, and the other on the outer equator of the plasma ($\Delta\phi$ = 180°, $\Delta\theta$ = 90°). The poloidal array consists of 2 × 5 b_θ-probes in the same poloidal plane, one at the top and the other at the bottom of the rectangular vacuum vessel, with an angular separation of $\Delta\theta$ = 10° (4 cm) between probes. Although located in the limiter shadow at r = 23 cm, the probes are placed in ceramic tubes at atmospheric pressure. In addition to allowing triple probe measurements without any problem of high-frequency cut-off associated with a metallic casing, the design allows the possibility to displace, rotate or change easily the magnetic probes. This flexibility has been greatly exploited in the present studies. The probes typically occupy a volume of 4 cm^3 giving a spatial resolution of about 1.6 cm. Each probe consists of 22 windings connected symmetrically to a bifilar cable that leads to a ferrite core transformer to reject a possible common mode. It is easy to check whether there still exists any capacitive coupling with the scrape-off plasma in this system: this is done by shunting the probe leads, thereby transforming the magnetic probe into an electrostatic probe. Such a test has been conducted and has shown that capacitive coupling is negligible for the measurements presented in this paper.

Density fluctuations are measured with an imaging diagnostic based on the phase contrast method [11,12]. It uses a 23 cm × 4 cm wide, 8 watt CO_2 laser beam transmitted through the plasma, producing an image of the plasma with the small phase shifts ($\tilde{\phi} \lesssim 10^{-3}$) due to refractive index perturbations being revealed as corresponding intensity variations. This diagnostic allows the study of a broad range of fluctuation wavelengths, between 0.2 and 20 cm with a sensitivity better than 10^{-5} radians for 1 MHz bandwidth, yielding line-integrated density fluctuations along selected vertical chords. More than half the plasma cross-section, centered on the low field side, is accessible with the available window. The chords are selected by displacing the detectors in the image plane.

In the scrape-off layer, density fluctuations are measured locally by a radially moveable Langmuir probe. The probe consists of three tips which allow to measure simultaneously fluctuations in the floating potential and ion saturation current [13]. This provides the possibility of poloidal coherence and fluctuation-induced transport measurements [14,15].

The signals from each of the above diagnostics are analysed in two ways. Firstly, they can be stored in an 8 channel, 8 bit, 64 K CAMAC acquisition system sampling at 1 MHz, for the use of digital Fourier and correlation analysis. Secondly, a series of eight passive bandpass filters with half-octave wide bands geometrically spaced between 50 and 560 kHz, can be used to yield good time resolved spectral measurements.

RESULTS

Each of the three diagnostics measures a fluctuating signal that is characterized by a broadband incoherent spectrum above the Mirnov frequency. Mirnov oscillations, produced by the rotation of a macroscopic magnetic structure, result in a coherent peak ($\Delta\omega/\omega \ll 1$) at a frequency of about 15 kHz.

Comparison of Spectra

All three diagnostics yield power spectra decreasing with $f^{-\alpha}$ above a roll-off frequency f_c. For the magnetic power spectra (Fig. 2a), $\tilde{b}_\theta$ and $\tilde{b}_r$ exhibit a similar slope at higher frequencies. Their level also is similar, taking into account the effect of the wall. The level of the magnetic fluctuations, measured 4 cm behind the limiter, is in the range $[\tilde{b}_\theta(f > 40\ \text{kHz})/B_\theta] = 10^{-4} - 10^{-5}$.

Line-integrated profiles of density fluctuations determined from the phase contrast diagnostic, while being usually rather flat or slowly increasing towards the edge for low frequencies ($f < 100$ kHz), are somewhat peaked at higher frequencies ($f > 100$ kHz). The relative fluctuation level is estimated to be $\tilde{n}_e/n_e \simeq 10\%$ for $r/a = 0.75$. Spectra measured from a central chord are broader than those obtained from an edge chord (Fig. 2b). Figure 3 shows that the roll-off frequency f_c gradually decreases from a central chord ($\sim$ 150 kHz) to lower values for edge chords ($f_c < 100$ kHz). The edge chord spectrum is very similar to the ion saturation current spectrum measured by the Langmuir probe in the scrape-off layer (Fig. 2c). The Langmuir probe measures a high level of density fluctuations, $\tilde{n}_e/n_e \simeq$ 50-100%, following the usual trend of increasing density fluctuations towards the plasma edge. Figure 3 also shows that the spectral index α of density fluctuations (above the roll-off frequency) is only weakly dependent on position.

In comparison, the magnetic fluctuations $\tilde{b}_\theta$ show spectral index values which do not appreciably differ from density fluctuation data. Furthermore, under ohmic heating conditions, the spectral indices of the density and magnetic fluctuations are not very sensitive to changes in the plasma parameters.

Scaling with Plasma Parameters

We have reported previously that magnetic fluctuations scale inversely with the electron confinement time in ohmic discharges, suggesting a possible relation with confinement [7,9]. In the latter study with SiC-coated carbon limiters, the toroidal field and the plas-

ma current and density were varied over a wide range: B_ϕ = 0.78, 1.16, 1.51 T; 40 < I_p < 150 kA (2.6 < q(a) < 15); 1.5 < $\bar{n}_e$ < 9 10^{19} m^{-3}. Preliminary to this study, we had investigated the effect of transient $\bar{n}_e$ and I_p (both increasing and decreasing) on the level of magnetic fluctuations. This was undertaken, for example, by varying the density ramp around a fixed density while maintaining at the same time a fixed current. A positive density ramp was found to reduce the level of fluctuations over the whole spectrum, while a positive current ramp increased the level. These measurements permit us to delimit the tolerable range of stationary conditions around $\dot{\bar{n}}_e = \dot{I}_p = 0$ for the use in such a parameter scan. At the same time, these measurements indicate a sensitivity of the magnetic fluctuations on the width of the plasma current channel.

It has been found that the amplitude of the magnetic fluctuations scale as

$$\frac{\tilde{b}_\theta}{B_\theta(a)} \sim \left(B_\phi \bar{n}_e^{1/2}\right)^{-1} \sim \tau_{Ee} \ ,$$

exhibiting a strong dependence on the plasma current [9].

In contrast with magnetic fluctuations, density fluctuations measured along a central chord, yield a very different scaling:

$$\tilde{\bar{n}}/\bar{n}_e \sim \text{const.}$$

No systematic plasma current dependence was found, with a completely opposite trend being observed when $\bar{n}_e$, and therefore τ_{Ee}, was increased [14]. We therefore conclude that the measured density and magnetic fluctuations follow completely different scalings, indicating likely differences in their nature and origin.

Poloidal Correlations of Density Fluctuations

Correlation measurements using Langmuir probes yield poloidal phase velocities in the range of 1-5 10^3 m/sec (ion diamagnetic direction). By correlating measurements from two adjacent chords of the phase contrast diagnostic, one obtains phase velocities of the order of 2 10^3 m/sec for r/a > 0.7 and up to 5 10^3 m/sec for r/a < 0.7 (undetermined direction). Significant coherence has been found over sizable poloidal distances using the phase contrast diagnostic. Figures 4a and 4b show the spatial autocorrelation function of the density fluctuation, obtained by plotting the real part of the cross-power at chosen frequencies, between signals from two scannable detectors. For frequencies up to 100 kHz, sizable coherence is observed between chords separated by up to 7 cm. We define a mean wavelength $\Lambda_{mean} = 2\pi/k_{mean}$, deduced from the oscillation period of the spatial autocorrelation function, which is to be understood in a statistical sense. This allows a statistical dispersion curve to be drawn. Figure 5 shows the curve obtained when the central chord is taken as the reference. The wavenumber for this case should be interpreted as k_Θ rather than k_r. The slope of the line shown in Fig. 5 yields a phase velocity of the same order as the electron diamagnetic drift speed $v_{De} = \nabla p/en_e B_T \simeq 5\ 10^3$ m/sec. For a reference edge chord, with the measurements then providing an indication of k_r, smaller phase velocities are obtained, as can be inferred from Fig. 4b.

More than half of the spectral power has been measured to be associated with long wavelengths, that is in the region $k\ \rho_s = k\ c_s/\omega_{ci} < 0.3$ (central chord). These values are comparable to those predicted by strong drift wave models [1]. In terms of the poloidal wavenumber, this corresponds to

$m_{mean} = k_{\Theta mean}\ r = 2\pi r/\Lambda_{mean} \simeq 20$ at r/a = 0.75 and f = 100 kHz.

It should be stressed that m_{mean} by definition arises from the spatial autocorrelation function and is not to be understood in the sense of a global coherent mode.

Similarly, at the edge, the ion saturation current fluctuations measured by the Langmuir probe show also half of the fluctuation spectral power at very long wavelength, that is for $k\rho_s < 0.1$. These long wavelengths correspond to low frequencies ($f < 80$ kHz), for which most of the linear particle transport $\langle \underline{\tilde{n}} \cdot \underline{\tilde{E}} \rangle$ has been measured to occur (Fig. 2c) [14,15]. (It should be noted that the relation between the particle transport and the heat transport is not obvious.)

Magnetic Fluctuations Geometry

1) Anisotropy of the Magnetic Field Fluctuations

In the early work of Ivanov et al. [16] on broadband magnetic fluctuations in the T-4 tokamak, it was found that $\tilde{b}_\phi$ fluctuations were of much smaller amplitude than $\tilde{b}_\theta$ fluctuations. Profiting from the flexibility of design of our edge magnetic probe system, we have continuously rotated a "b_θ-probe" from its original angular position to an angle at which it is only sensitive to toroidal field fluctuations. The probe direction has been calibrated by zeroing the probe signal due to the main B_ϕ field in the absence of a toroidal plasma current. For all the frequencies analysed using the series of eight bandpass filters monitoring the broadband spectrum, the fluctuation amplitude passes through a sharp minimum close to, but different from, the toroidal direction. An example of such an angular scan is shown in the insert of Fig. 6. At the angle of this sharp minimum, the signal decreases to typically 10^{-2} of the maximum value near the poloidal direction. This small value might possibly be reduced by a more acute alignment of the effective probe surface.

By varying the current, and for two toroidal field directions, we find that this minimum is aligned with the total field at the probe position [14]. This strong anisotropy of the fluctuating fields in the direction perpendicular to the static field indicates that the fluctuating currents associated with the broadband magnetic fluctuations oscillate parallel to the total magnetic field.

2) Multipolar Field Decay

A possible method of measuring the mean poloidal wavenumber m_{mean} of broadband magnetic fluctuations is to assume that the field associated with fluctuating plasma currents decays like a multipolar vacuum field for radii larger than the plasma radius a. In addition, it is to be assumed that no local $\tilde{b}$ is produced in the scrape-off layer, $r > a$. For a cylindrical plasma, this yields

$$\tilde{b}_\theta(r>a) \sim \frac{1+\left(\frac{r}{r_w}\right)^{2|m|}}{\left(\frac{r}{a}\right)^{|m+1|}}$$

where r_w is the wall radius. In fact, the measured signal would be the result of a sum over different m-modes, however, it is not possible with these measurements to determine the mode distribution. One will therefore obtain a mean poloidal wave number m_{mean}.

Figure 7 shows the result of a radial scan with a b_θ-probe, the results being displayed for three different frequencies. By comparing the measurements with the results of the model calculation and taking into account the finite size of the probe, an estimate of m_{mean} is obtained. Typically, one finds $6 \leq m_{mean} \leq 8$ at 280 kHz. Figure 7 indicates that m increases with frequency. These results are also plotted in Fig. 5, indicating a dispersion relation that is very different from that obtained for the density fluctuations.

3) Spatial Correlations

The coherence $|P_{12}/\sqrt{P_{11}}\sqrt{P_{22}}|$ between signals from different probes gives some indications of the geometry of the perturbed magnetic fields.

Firstly, it is instructive to correlate the signals obtained from two probes b_r and b_θ at the same spatial position, occupying the same volume. A typical example is shown in Fig. 8. No significant coherence is observed for the broadband spectrum above 100 kHz. On the

other hand, the Mirnov harmonics region is characterized by a significant level of coherence. Mirnov harmonics peaks up to the sixth harmonic are visible in the coherence. The coherence level decreases gradually with frequency from about one at 15 kHz to a non-significant level at 100 kHz, while maintaining a constant phase relation. In general, the presence of strong Mirnov activity at 10-15 kHz increases the fluctuation level in the bandpass filters centered at 50 and 70 kHz, and is evident in the power spectrum for frequencies up to typically 100 kHz. These observations indicate that one should conceptually and experimentally distinguish the Mirnov harmonics region from the higher frequency region of the turbulent spectrum.

The lack of coherence observed between $\tilde{b}_r$ and $\tilde{b}_\theta$ at the same location for higher frequencies, above typically 100 kHz, is an indication that $\tilde{b}_r$ and $\tilde{b}_\theta$ at the same spatial position are produced by different uncorrelated fluctuating currents $\tilde{j}_\parallel$ flowing at different plasma locations.

By correlating different neighbouring b_θ probes in a poloidal plane (Fig. 9), one observes that the coherence decreases with increasing poloidal spacing. Sizable coherence is measurable up to typically 30° spacing. The spatial autocorrelation function is shown in Fig. 4c. A typical wavelength is defined in a similar fashion as for the density fluctuations. This allows the measurement of mean poloidal wavenumbers by a second, independent method. The results obtained compare favourably with those determined from the study of the multipolar field decay using the vacuum field model (Fig. 5).

The slope of the statistical dispersion curve shown in Fig. 5 is 10^5 m/sec. This corresponds to a poloidal phase velocity 20 times higher than that obtained for the density fluctuations.

The coherence between $\tilde{b}_\theta$ signals obtained from far distant probes has also been investigated. Surprisingly, sizable coherence is found for a poloidal spacing $\Delta\theta \sim 180^\circ$ (Fig. 9). This corresponds to a much larger distance than the short coherence length described above ($\Delta\theta \sim \pm 30^\circ$). Significant coherence has also been found between signals from far distant magnetic probes separated by as much as ($\Delta\phi = 180^\circ$,

$\Delta\theta = 90^{\circ}$), as shown in Fig. 9 [14,17]. The probes used to obtain these results were aligned along the q = 2, 6,... magnetic field helicities.

These results firstly show that very long coherent structures exist along the torus, presumably along the magnetic field lines. Secondly, for the standard q = 3.2 discharge used, the q = 6 helicity is markedly outside the vacuum vessel, indicating that the measured coherence originates from the q = 2 helicity, a surface deep inside the plasma [14]. This suggests that magnetic fluctuations measured at the plasma edge in the scrape-off layer, carry information originating from the confining zones of the plasma. It is interesting that at the plasma edge the fluctuations are aligned along the static field at the edge (probe rotation experiment), whereas the above results indicate the existence of coherent structures aligned along field lines in the bulk plasma. This seems to speak in favour of a transport model where helical turbulent perturbations of the bulk plasma lead to the observed coherent perturbations at the edge.

DISCUSSION AND CONCLUSIONS

The detailed measurements of broadband density and magnetic fluctuations presented in this paper illustrate the existence of many important distinguishing features.

The scaling of the fluctuation amplitude with plasma parameters has been examined under ohmic conditions. Density fluctuations increase in amplitude with density, and thus with electron confinement time in the Alcator regime. For the same conditions, magnetic fluctuations on the contrary decrease with electron confinement time, showing perhaps more evidence of a link with confinement.

The phase contrast diagnostic, capable of measuring very long wavelengths, has shown that more than half of the spectral power in the bulk plasma is associated with very long wavelengths, $k \rho_s < 0.3$, as predicted by strong drift wave theory. This result is supported by the same conclusion obtained from edge plasma measurements using Langmuir probes, which also show that the linear transport is dominated by the low frequency, long wavelength contributions.

Magnetic fluctuations show long distance coherent structures aligned along field line helicities of the bulk plasma, as shown by the long distance toroidal and poloidal correlation measurements. In particular, our results indicate that the q = 2 helicity contributes to the measured coherence.

The very high coherence found along field lines, in contrast with the short poloidal coherence length, is indicative of waves propagating parallel to the magnetic field. Very low poloidal wavenumbers have been measured, e.g. $2 \leq m_{mean} \leq 7$ for frequencies in the range of 100 to 400 kHz, using two independent methods. We have thus been able to show, for the first time, the statistical dispersion relation for magnetic broadband turbulence. This yields a poloidal phase velocity of 10^5 m/sec, which corresponds to a toroidal phase velocity $v_\phi = v_\theta/tg\alpha \simeq 10^6$ m/sec $\simeq v_\parallel$, assuming the observed flute-like structure. This velocity is not much less than the characteristic Alfvén speed on axis $v_A = 4\ 10^6$ m/sec. The measured anisotropy of magnetic fluctuations with a large predominance of $\tilde{b}_\perp$ over $\tilde{b}_\parallel$, together with the strong coherence associated with the propagation along the field lines, are two typical characteristics of Shear Alfvén Waves.

In conclusion, we have determined the geometrical and temporal characteristics of broadband density and magnetic fluctuations, and have measured their scaling with plasma parameters and confinement. The evidence of differences in the characteristics observed between density and magnetic fluctuations indicate that they are associated with different physical phenomena.

ACKNOWLEDGEMENTS

The authors are grateful for the support of other members of the TCA team. It is also a pleasure for one of the authors (A. P.) to acknowledge discussions with P.A. Duperrex and M. Malacarne and to acknowledge stimulating discussions with F. Troyon. This work was partly supported by the Swiss National Science Foundation.

REFERENCES

[1] P.C. Liewer, Nucl. Fusion 25 (1985) 543.

[2] E. Mazzucato, Phys. Rev. Lett. 48 (1982) 1828.

[3] Equipe TFR, Plasma Phys. 25 (1983) 641.

[4] C.M. Surko and R.E. Slusher, Science 221 (1983) 817, and references therein.

[5] S.J. Zweben and R.J. Taylor, Nucl. Fusion 21 (1981) 193.

[6] B.A. Carreras et al., Phys. Rev. Lett. 50 (1983) 503.

[7] P.A. Duperrex et al., Phys. Lett. 106A (1984) 133.

[8] P.A. Duperrex, R. Keller, M. Malacarne, A. Pochelon, Proc. 12th EPS Conf. on Contr. Fusion and Plasma Phys., Budapest Vol. I (1985) 126.

[9] M.L. Sawley, A. Pochelon, R. Keller, ibid, Vol. I (1985) 291.

[10] B.B. Kadomtsev, Comments on Plasma Phys. 9 (1985) 227, and N. Ohyabu and J.K. Lee, General Atomic Report GA-A17890, November 1985.

[11] H. Weisen, Infrared Physics 25 (1985) 543.

[12] H. Weisen et al., Plasma Phys. and Contr. Fusion (1986) in press.

[13] A. de Chambrier et al., J. Nucl. Mat. 128&129 (1984) 310.

[14] Ch. Hollenstein et al., Proc. 13th EPS Conf. on Contr. Fusion and Plasma Heating, Schliersee, Vol. I (1986) 144.

[15] Ch. Hollenstein, Y. Martin and W. Simm, J. Nucl. Mat. (in press).

[16] N.V. Ivanov, I.A. Kovan and I.B. Semenov, Sov. J. Plasma Phys. 3(5) (1977) 526.

[17] M.L. Sawley et al., Bull. Am. Phys. Soc. 30 (1985) 1441.

FIGURE CAPTIONS

Fig. 1: Diagnostic layout of the TCA tokamak.

Fig. 2: Power spectra from
a) magnetic probes b_θ and b_r
b) chord-averaged density fluctuations
c) Langmuir probe ion saturation current

Fig. 3: Radial profile of the power spectral index of the density fluctuations. The vertical bar represents the value for $\tilde{b}_\theta$ measured at the indicated position, although the signal is not local.

Fig. 4: The spatial autocorrelation function of fluctuations in a poloidal plane: for density fluctuations along (a) a central chord, (b) an edge chord; and for (c) magnetic field fluctuations.

Fig. 5: Statistical dispersion relation for density and magnetic fluctuations.

Fig. 6: Anisotropy of the magnetic field fluctuations in a plane tangential to the plasma surface (top left insert), and angular position α_{min} of the minimum fluctuation amplitude for different plasma currents and $\pm B_\phi$.

Fig. 7: Radial dependence of the amplitude of the poloidal magnetic field fluctuations in the scrape-off layer.

Fig. 8: Coherence and phase between signals from two probes b_r and b_θ located at the same position.

Fig. 9: Long distance poloidal and toroidal coherence.

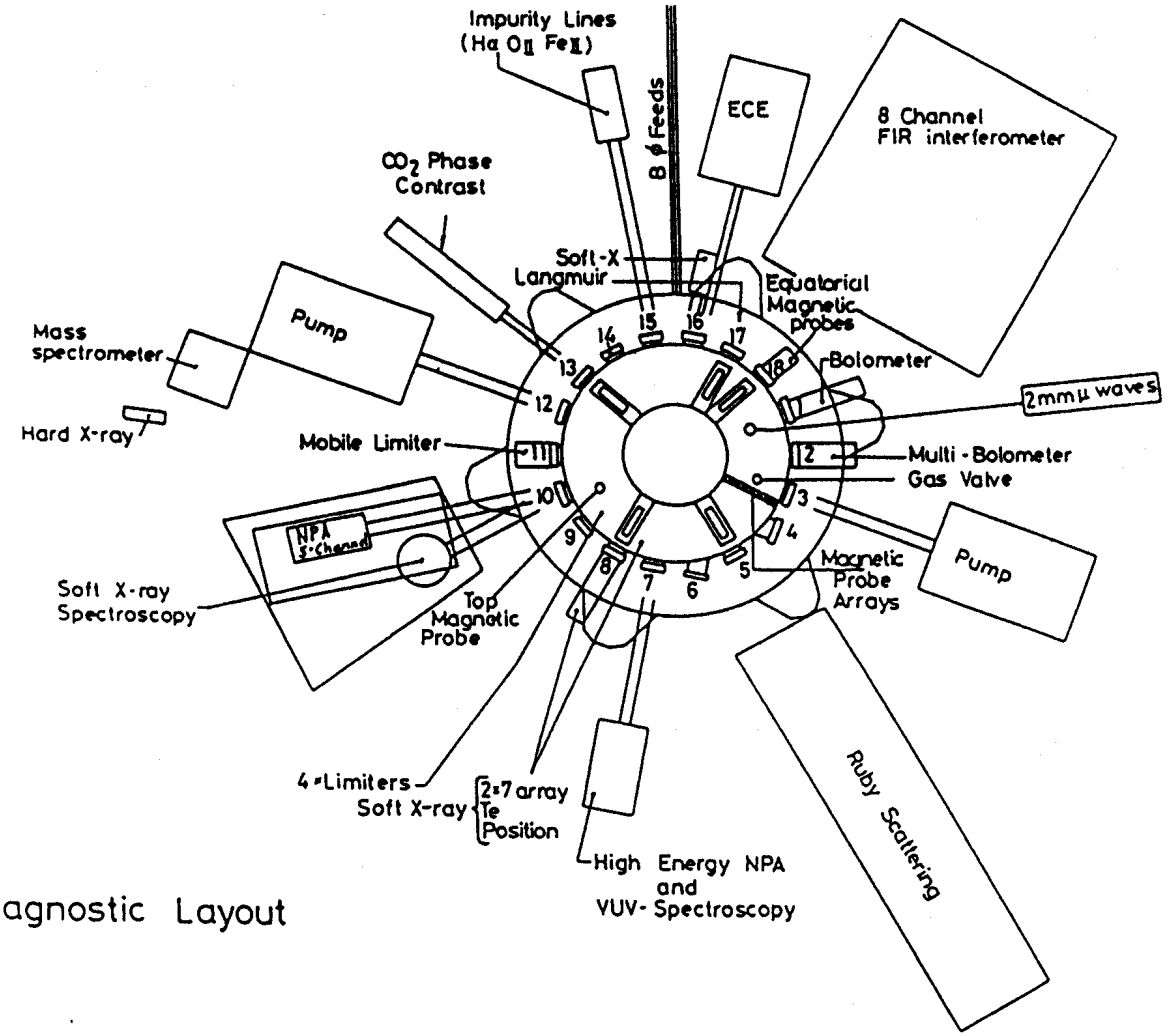

Diagnostic Layout

FIG. 1

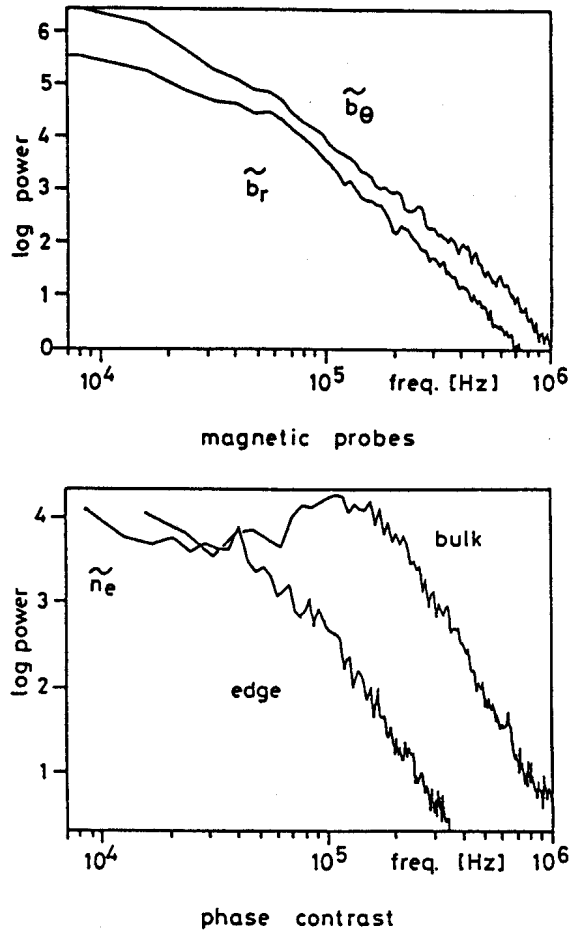
log power
$\tilde{b}_\theta$
$\tilde{b}_r$
freq. [Hz]
magnetic probes
A)
$\tilde{n}_e$
bulk
edge
phase contrast
B)

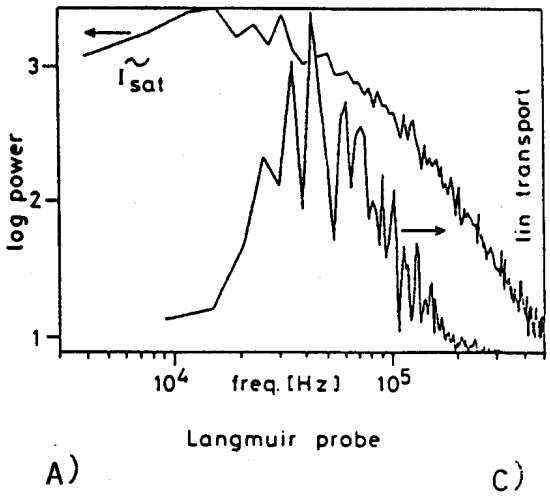
log power
$\tilde{I}_{sat}$
lin transport
freq. [Hz]
Langmuir probe
C)

FIGS. 2

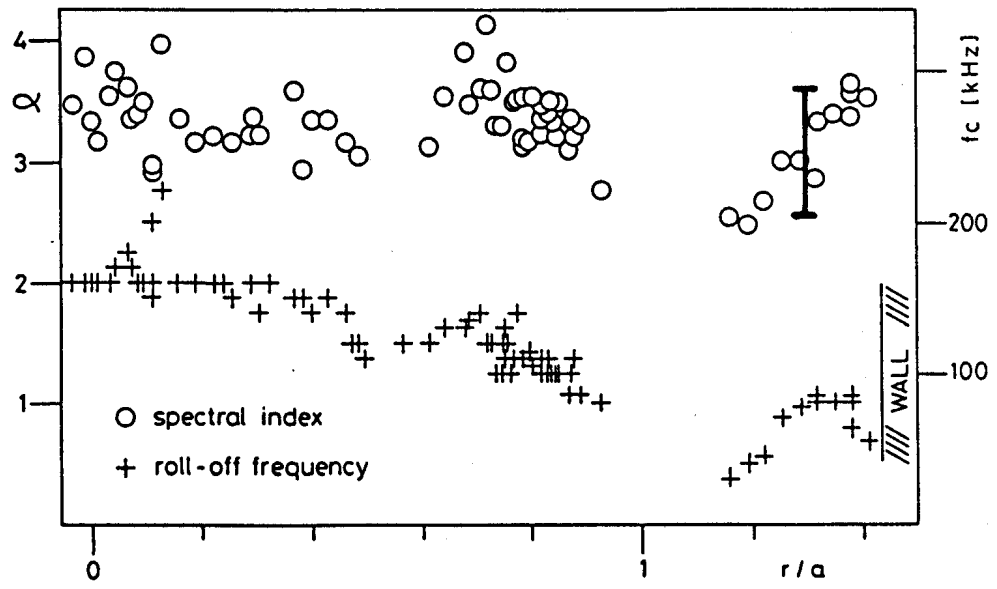
α
fc [kHz]
200
100
WALL
O spectral index
+ roll-off frequency
r/a

FIG. 3

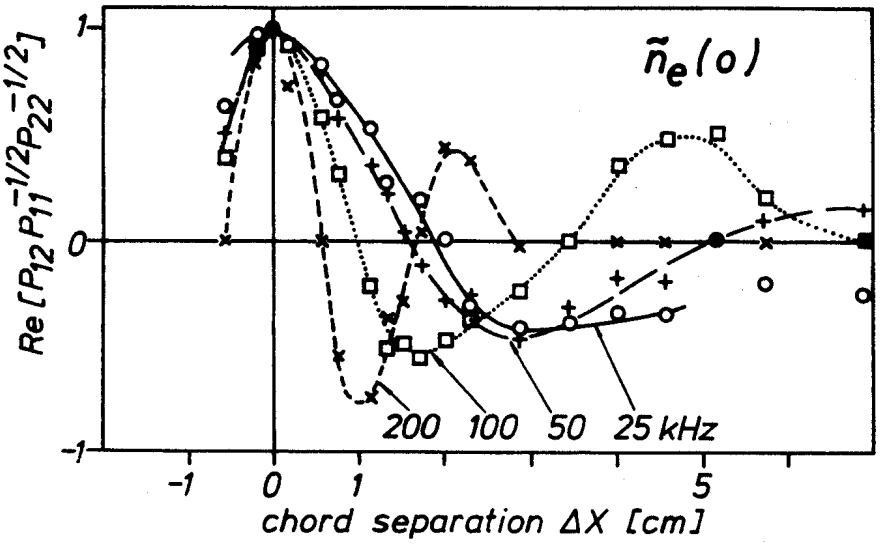
$\tilde{n}_e(o)$
200
100
50
25 kHz
Re $[P_{12}P_{11}^{-1/2}P_{22}^{-1/2}]$
chord separation ΔX [cm]

A)

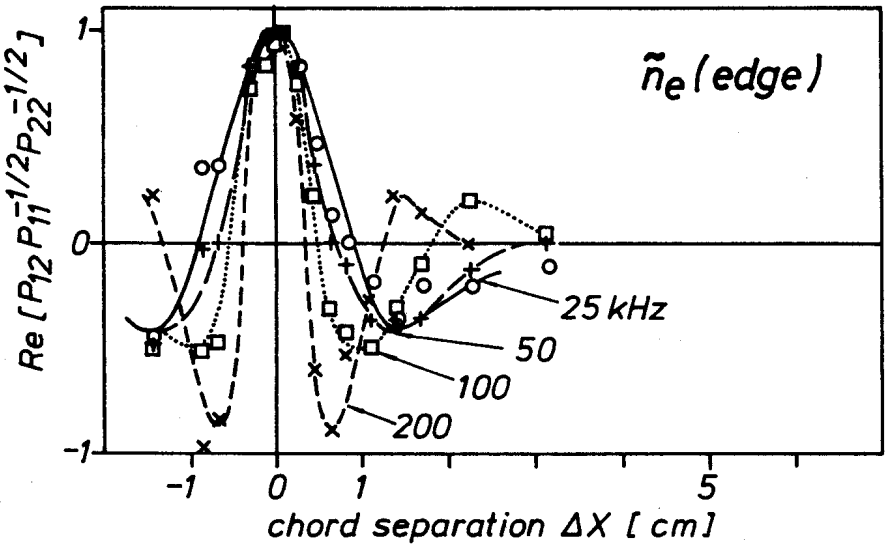
$\tilde{n}_e$ (edge)
25 kHz
50
100
200
Re $[P_{12}P_{11}^{-1/2}P_{22}^{-1/2}]$
chord separation ΔX [cm]

B)

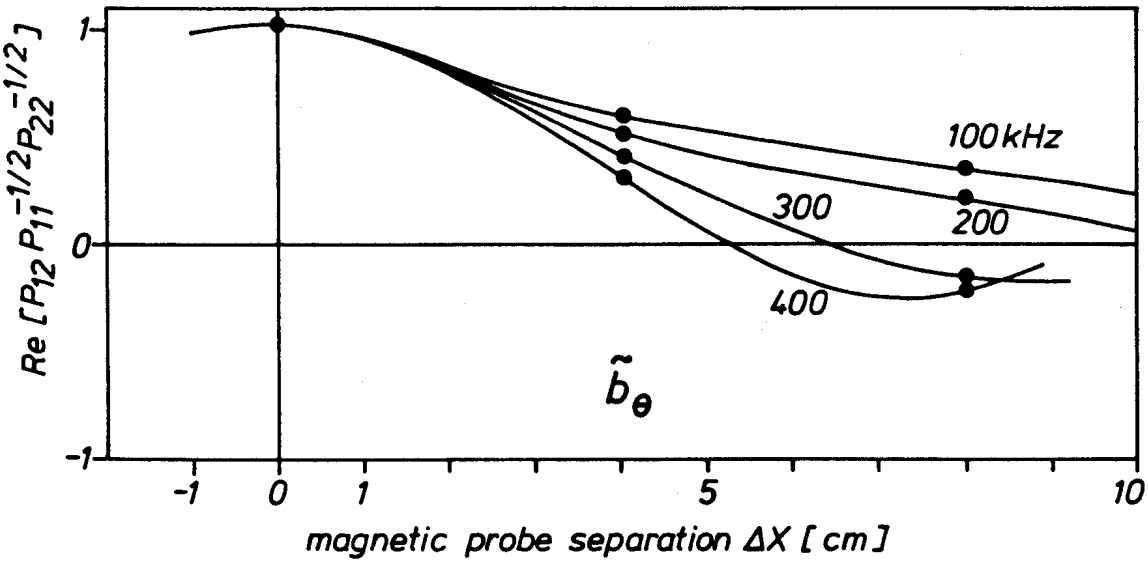
100 kHz
300
200
400
$\tilde{b}_\theta$
Re $[P_{12}P_{11}^{-1/2}P_{22}^{-1/2}]$
magnetic probe separation ΔX [cm]

C)

FIGS. 4

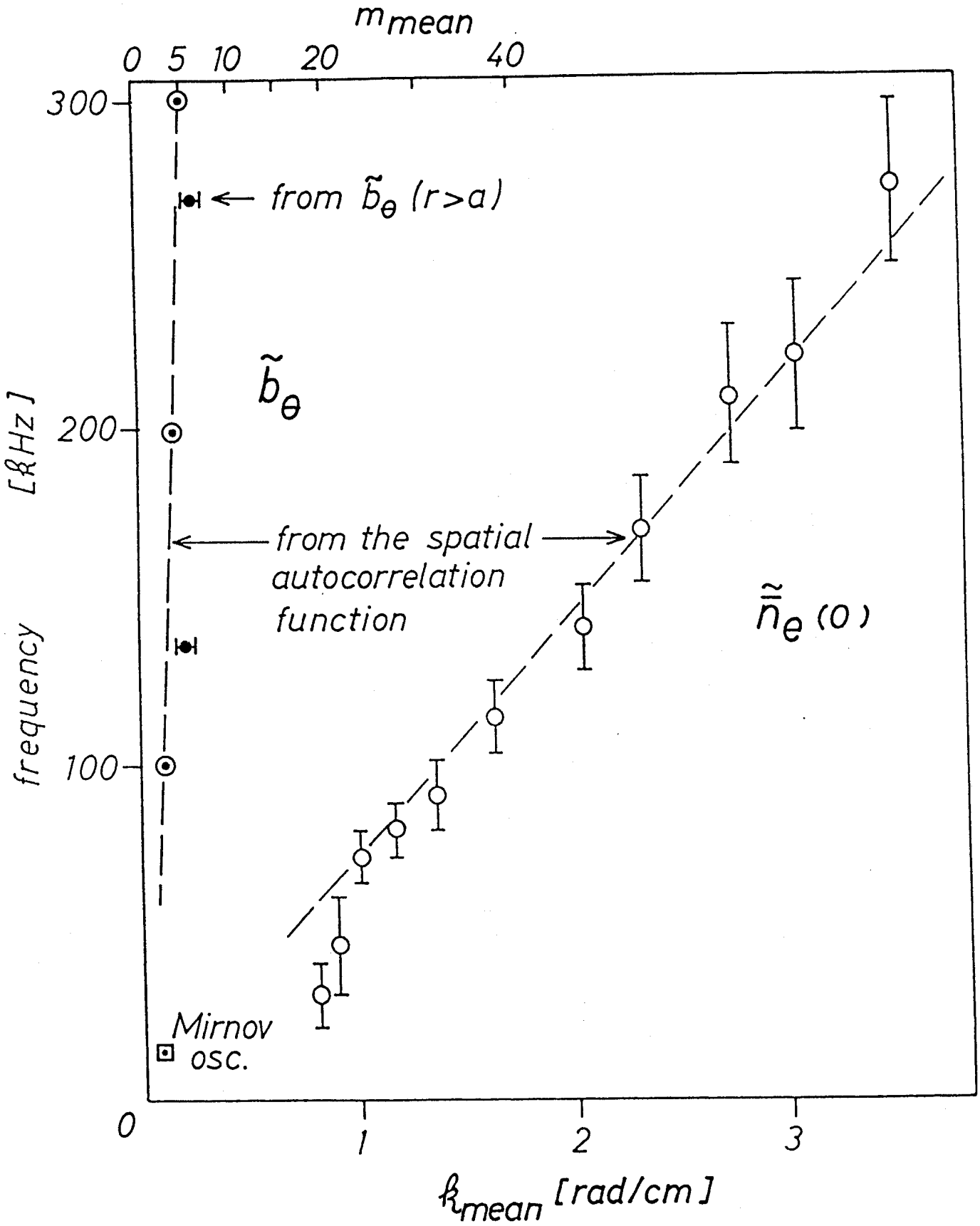
m_{mean}
0 5 10 20 40
300
200
100
0
frequency [kHz]
← from $\tilde{b}_\theta$ (r>a)
$\tilde{b}_\theta$
from the spatial autocorrelation function
$\tilde{\tilde{n}}_e$ (0)
Mirnov osc.
1
2
3
k_{mean} [rad/cm]

FIG. 5

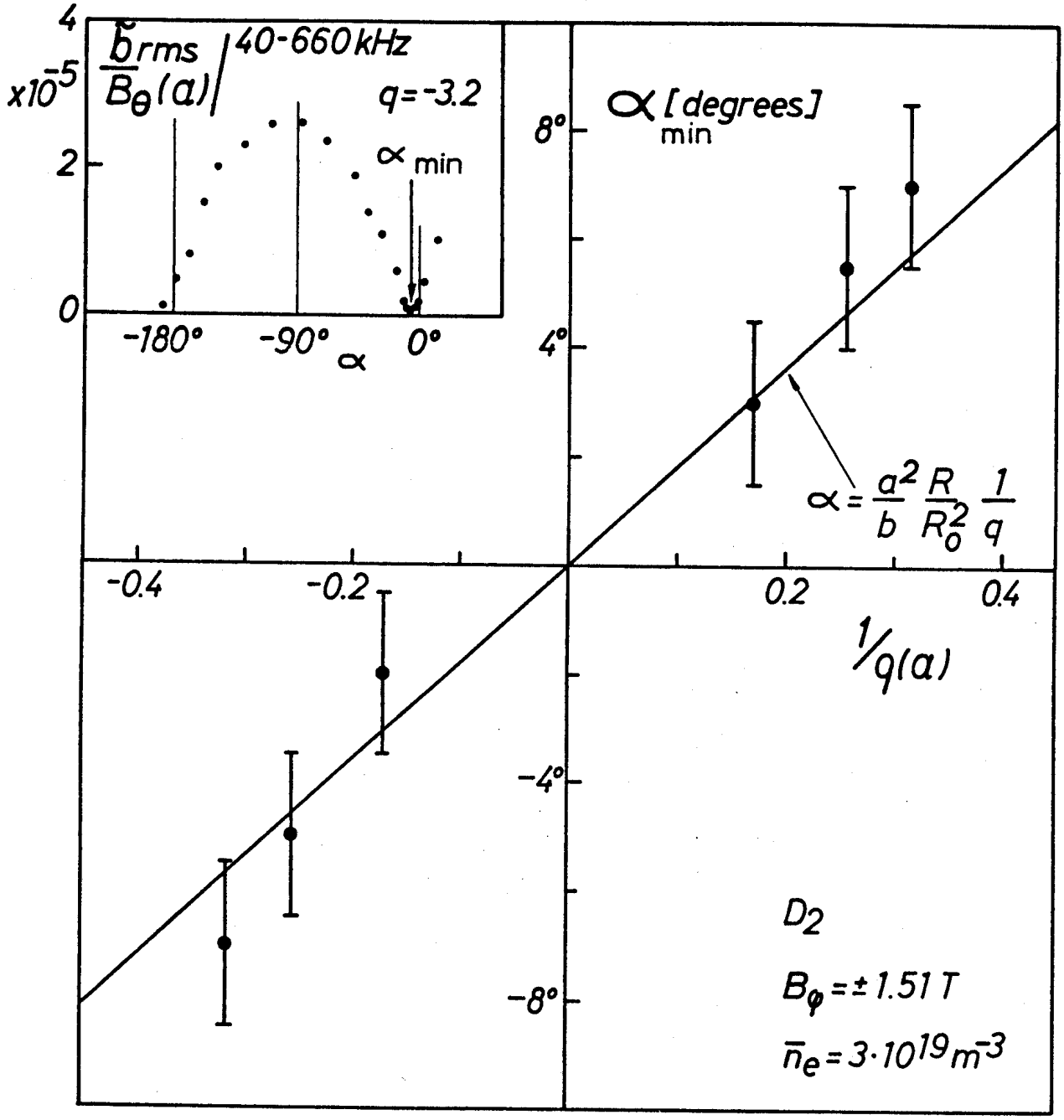
4
x10⁻⁵
2
0
b̃rms / Bθ(a)
40-660 kHz
q=-3.2
α min
-180°
-90°
α
0°
α [degrees]
min
8°
4°
-4°
-8°
-0.4
-0.2
0.2
0.4
1/q(a)
α = a²/b R/R₀² 1/q
D2
Bφ = ± 1.51 T
n̄e = 3·10¹⁹ m⁻³

FIG. 6

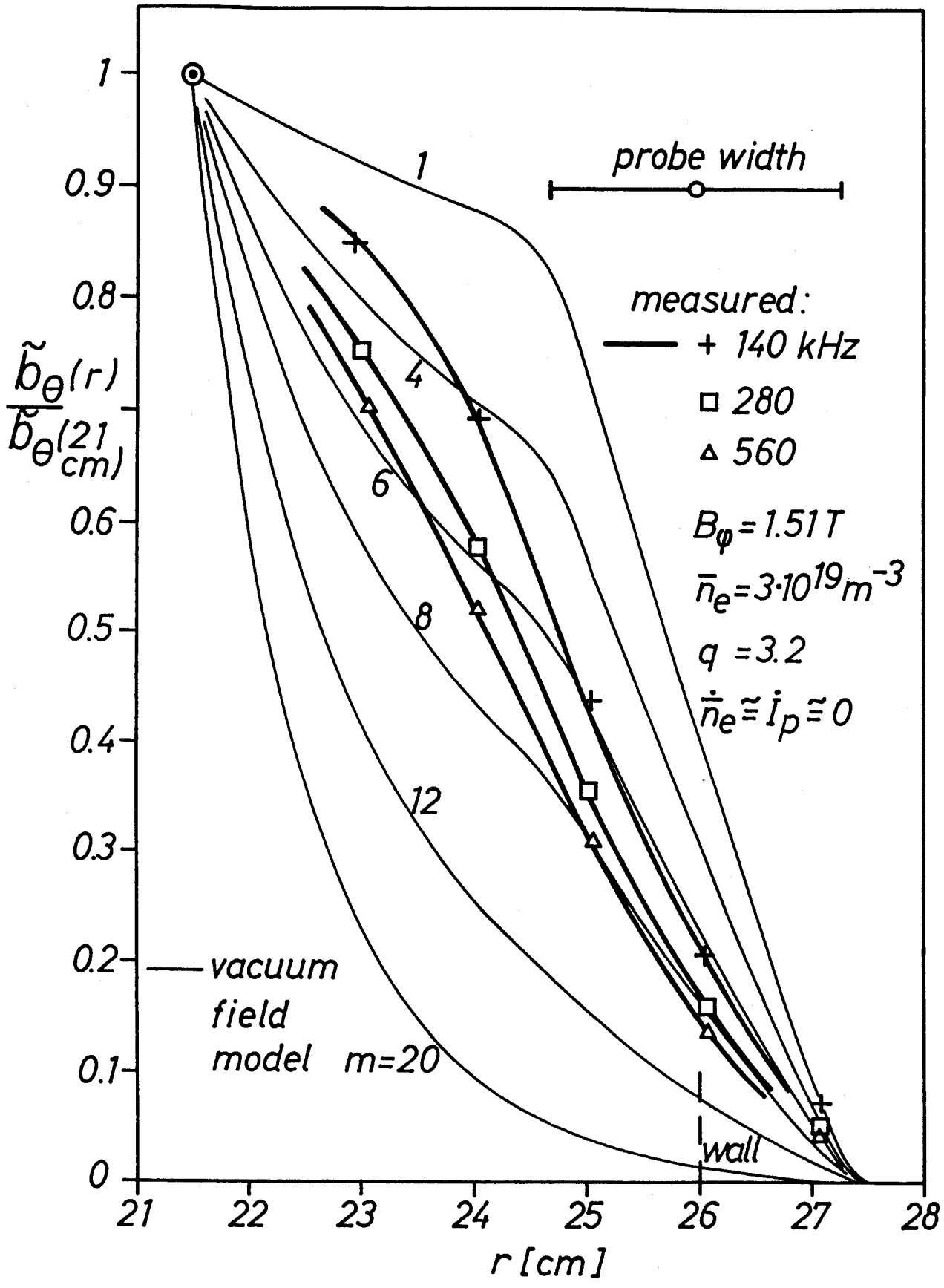
1
0.9
0.8
0.6
0.5
0.4
0.3
0.2
0.1
0
$\frac{\tilde{b}_\theta(r)}{\tilde{b}_\theta(21\,cm)}$
1
4
6
8
12
probe width
measured:
+ 140 kHz
□ 280
△ 560
$B_\varphi = 1.51\,T$
$\bar{n}_e = 3 \cdot 10^{19} m^{-3}$
$q = 3.2$
$\dot{\bar{n}}_e \cong \dot{I}_p \cong 0$
vacuum field model m=20
wall
21
22
23
24
25
26
27
28
r [cm]

FIG. 7

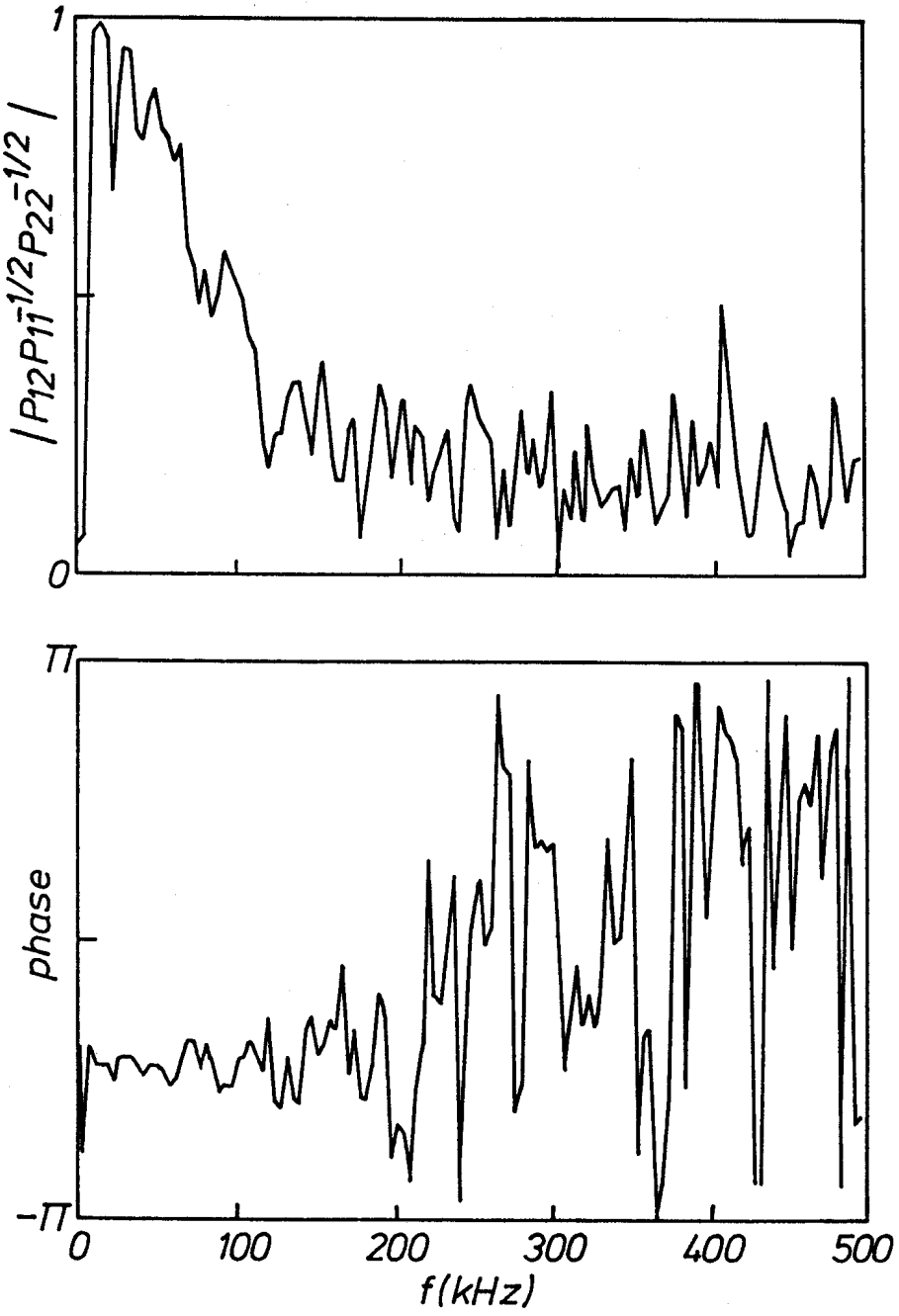

FIG. 8

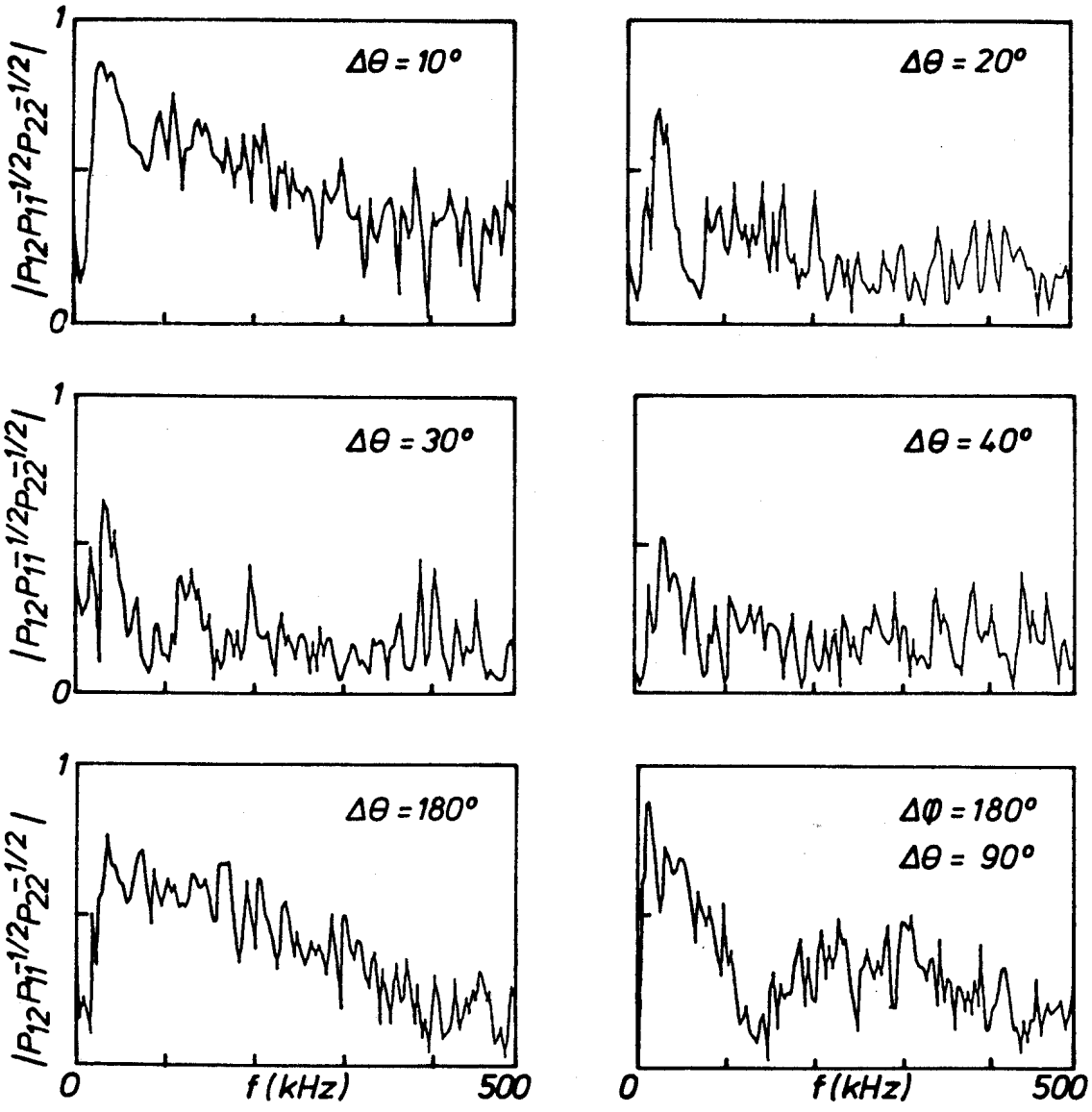
1
0
$|P_{12}P_{11}^{-1/2}P_{22}^{-1/2}|$
Δθ = 10°
Δθ = 20°
Δθ = 30°
Δθ = 40°
Δθ = 180°
Δφ = 180°
Δθ = 90°
0
f (kHz)
500

FIG. 9